Ultrabroadband Supercontinuum Generation and Frequency-Comb Stabilization Using On-Chip Waveguides with Both Cubic and Quadratic Nonlinearities

Daniel D. Hickstein,[1,*] Hojoong Jung,[2] David R. Carlson,[1] Alex Lind,[1,3] Ian Coddington,[4] Kartik Srinivasan,[5] Gabriel G. Ycas,[1] Daniel C. Cole,[1,3] Abijith Kowligy,[1] Connor Fredrick,[1,3] Stefan Droste,[4] Erin S. Lamb,[1] Nathan R. Newbury,[4] Hong X. Tang,[2] Scott A. Diddams,[1,3] and Scott B. Papp[1]

[1]*Time and Frequency Division, National Institute of Standards and Technology, Boulder, Colorado 80305, USA*

[2]*Department of Electrical Engineering, Yale University, New Haven, Connecticut 06520, USA*

[3]*Department of Physics, University of Colorado, Boulder, Colorado 80309, USA*

[4]*Applied Physics Division, National Institute of Standards and Technology, Boulder, Colorado 80305, USA*

[5]*Center for Nanoscale Science and Technology, National Institute of Standards and Technology, Gaithersburg, Maryland 20899, USA*

(Received 12 April 2017; published 24 July 2017)

Using aluminum nitride photonic-chip waveguides, we generate optical-frequency-comb supercontinuum spanning from 500 to 4000 nm with a 0.8-nJ seed pulse, and we show that the spectrum can be tailored by changing the waveguide geometry. Since aluminum nitride exhibits both quadratic and cubic nonlinearities, the spectra feature simultaneous contributions from numerous nonlinear mechanisms: supercontinuum generation, difference-frequency generation, second-harmonic generation, and third-harmonic generation. As one application of integrating multiple nonlinear processes, we measure and stabilize the carrier-envelope-offset frequency of a laser comb by direct photodetection of the output light. Additionally, we generate approximately 0.3 mW of broadband light in the 3000- and 4000-nm spectral region, which is potentially useful for molecular spectroscopy. The combination of broadband light generation from the visible through the midinfrared, combined with simplified self-referencing, provides a path towards robust comb systems for spectroscopy and metrology in the field.

DOI: 10.1103/PhysRevApplied.8.014025

I. INTRODUCTION

Optical frequency combs are laser-based light sources that enable a wide variety of precision measurements, including the comparison of state-of-the-art atomic clocks [1], the quantitative measurement of pollution over several-kilometer paths above cities [2,3], and even the search for distant Earth-like planets [4,5]. Laser frequency combs are typically generated with relatively narrow (about 10%) relative spectral bandwidth [6]. However, a broad bandwidth is a requirement for many applications, such as spectroscopy, where it is desirable to probe several atomic or molecular transitions simultaneously, and optical frequency metrology, where stable lasers at different wavelengths must be compared. Consequently, narrowband frequency combs are usually spectrally broadened to at least one octave via supercontinuum generation (SCG) in materials with cubic nonlinearity ($\chi^{(3)}$), such as highly nonlinear fiber (HNLF) or photonic-crystal fiber [7].

Moreover, octave-spanning bandwidth allows the carrier-envelope-offset frequency (f_{CEO}) of the frequency comb to be measured (and subsequently stabilized) using "f-2f" self-referencing [8–10]. In the f-2f scheme, the low-frequency portion of the spectrum undergoes second-harmonic generation (SHG) in a material with quadratic nonlinearity ($\chi^{(2)}$), such as $LiNbO_3$, and interferes with the high-frequency portion of the spectrum, producing a signal that oscillates at f_{CEO}. Because of the modest effective nonlinearity of silica HNLF, SCG using traditional silica fiber requires high peak powers (typically 10 kW or more), which increases the electrical power requirements of the laser and limits the achievable repetition rates. Indeed, the adoption of compact frequency-comb sources at gigahertz repetition rates, such as electro-optic combs [11,12] and microresonator combs [6,13,14], is currently hindered by the difficulty of generating octave-spanning spectra using low-peak-power pulses. In addition, many potential applications for frequency combs require supercontinuum light at wavelengths that are difficult to achieve with SCG in silica fiber. For example, light in the midinfrared (3- to 8-μm) region is advantageous for molecular spectroscopy [15–19], but it is absorbed by silica fiber.

Fortunately, on-chip photonic waveguides with wavelength-scale dimensions offer high confinement of light, which provides a substantial increase in the effective nonlinearity,

*danhickstein@gmail.com

$$\gamma = \frac{2\pi n_2}{\lambda A_{\text{eff}}}, \tag{1}$$

where λ is the wavelength, A_{eff} is the effective area of the mode, and n_2 is the material-dependent nonlinear index, which is directly proportional to $\chi^{(3)}$ [7]. In addition, materials with a higher $\chi^{(3)}$—such as silicon nitride [20–27], silicon [28–30], aluminum gallium arsenide [31], and chalcogenide materials [32,33]—further increase γ and allow much lower peak power (<1 kW) to be used for the SCG process. High-confinement waveguides provide the additional advantage of increased control over the group-velocity dispersion (GVD), and therefore the spectral output of the SCG process.

Currently, supercontinuum generation in materials with both strong $\chi^{(2)}$ and $\chi^{(3)}$ is opening alternative possibilities for broadband light sources. For example, experiments with periodically poled $LiNbO_3$ (PPLN) have demonstrated supercontinuum generation via cascaded $\chi^{(2)}$ processes, and the simultaneous generation of supercontinuum and harmonic light [34–36]. Recently, aluminum nitride (AlN) has emerged as a lithographically compatible material that exhibits both strong $\chi^{(2)}$ and $\chi^{(3)}$, in addition to a broad transparency window. Consequently, thin-film AlN is proving to be a versatile platform for nanophotonics, providing phase-matched SHG [37], frequency-comb generation [38], and ultraviolet light emission [39].

Here, we present our observations of SCG in lithographically fabricated, on-chip AlN waveguides and demonstrate that the platform provides exciting capabilities: (1) We observe SCG from 500 to 4000 nm, and we show that the spectrum can be tailored simply by changing the geometry of the waveguide. (2) We find that the material birefringence induces a crossing of the transverse-electric (TE) and transverse-magnetic (TM) modes, which enhances the spectral brightness in a narrow band, and that the spectral location of this band can be adjusted by changing the waveguide dimensions. (3) We observe bright SHG, which is phase matched via higher-order modes of the waveguide, as well as phase-mismatched difference-frequency generation (DFG), which produces broadband light in the 3500- to 5500-nm region. (4) We demonstrate that simultaneous SCG and SHG processes in an AlN waveguide allows f_{CEO} to be extracted directly from the photodetected output, with no need for an external SHG crystal, recombination optics, or delay stage. (5) We use this simple scheme to lock the f_{CEO} of a compact laser frequency comb, and we find that the stability of the locked f_{CEO} is comparable to a standard f-$2f$ interferometer and is sufficient to support precision measurements.

II. EXPERIMENT

The fully SiO_2-clad AlN waveguides [38,40] have a thickness (height) of 800 nm, and a width that varies from 400 to 5100 nm. Near the entrance and exit facets of the chip, the waveguide width tapers to 150 nm in order to expand the mode and improve the coupling efficiency, which is estimated at −4 dB/facet, on average. We generate the supercontinuum by coupling into the waveguide approximately 80 mW of 1560-nm light from a compact, turnkey Er-fiber frequency comb [41], which produces pulses of approximately 80 fs at 100 MHz. The polarization of the light is controlled using achromatic quarter and half wave plates. The light is coupled into each waveguide using an aspheric lens (NA = 0.6) designed for 1550 nm. For output coupling, two different techniques are used, as shown in Fig. 1(b). In the case of f_{CEO} detection, the light is outcoupled using a visible-wavelength microscope objective (NA = 0.85) and then dispersed with a grating before illuminating a photodiode. Alternatively, when recording the spectrum, the light is collected by butt coupling an InF_3 multimode fiber (NA = 0.26) at the exit facet of the chip. The waveguide output is then recorded using two optical spectrum analyzers (OSAs); a grating-based OSA is used to record the spectrum across the visible and near-infrared regions, while a Fourier-transform OSA extends the coverage to 5500 nm.

To model the supercontinuum generation, we perform numerical simulations using the nonlinear Schrödinger equation (NLSE), as implemented in the PyNLO package

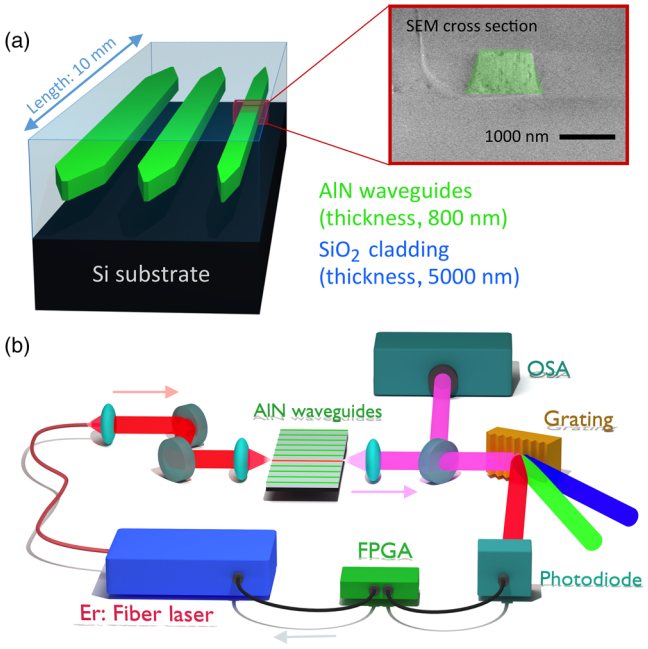

FIG. 1. (a) Aluminum nitride (AlN) on-chip waveguides embedded in SiO_2 tightly confine the light field, providing high nonlinearity. (b) To generate supercontinuum, 80-fs laser pulses (1560 nm, 800 pJ) are coupled into each waveguide. The broadband output is directed into an optical spectrum analyzer (OSA), or dispersed with a grating, where f_{CEO} is detected in the 780-nm region using a photodiode. The f_{CEO} signal is digitized using a field-programmable gate array (FPGA), which applies feedback to the laser pump diode.

[42–45]. The effective refractive indices and effective nonlinearities of the waveguides are calculated using the vector finite-difference mode solver of Fallahkhair *et al.* [46]. The NLSE includes $\chi^{(3)}$ effects and incorporates the full wavelength dependence of the effective index, but it does not take into account any $\chi^{(2)}$ effects, higher-order modes, or wavelength-dependent absorption. In the simulations, we use $n_2 = 2.3 \times 10^{-19}\,\mathrm{m}^2/\mathrm{W}$ for AlN [38], which is very similar to the value of $2.4 \times 10^{-19}\ \mathrm{m}^2/\mathrm{W}$ measured for silicon nitride [47].

III. RESULTS AND DISCUSSION

A. Supercontinuum from visible to midinfrared

When pumped in the lowest-order quasi-transverse-electric mode (TE_{00}), the AlN waveguides generate light (Fig. 2) from the blue portion of the visible region (approximately 500 nm) to the midinfrared (about 4000 nm). The broad peaks on both sides of the spectrum are the short- and long-wavelength dispersive waves [labeled SWDW and LWDW, respectively, in Figs. 2(b) and 2(c)], which are generated at locations determined by the GVD of the waveguide [7,48]. The broadband spectrum is a result of the flat GVD profile enabled by strong confinement of the light in these waveguides. The simulated spectra [Fig. 2(c)] reproduce the spectral location of the long- and short-wavelength dispersive waves. However, the NLSE simulations overestimate the light intensity in the dispersive waves compared to the experiment. One reason for this discrepancy is that the waveguide mode at 1560 nm does not have perfect overlap with modes at different wavelengths, and the effective nonlinearity is actually smaller than what is predicted by Eq. (1), which assumes perfect mode overlap. This effect is most pronounced at longer wavelengths, where the mode extends significantly outside of the waveguide and does not overlap well with the 1560-nm mode, which is mostly confined within the AlN waveguide.

When waveguide widths near 3500 nm are used, the supercontinuum shows high spectral intensity over a broad region from 1400 to 2800 nm, generally remaining within −20 dB of the transmitted pump intensity. This bright spectrum represents a promising source for molecular spectroscopy since OH-stretching transitions absorb in this region [49]. Indeed, sharp dips visible in the spectral intensity near 2700 nm are due to the absorption of water vapor in the OSA. Unfortunately, a sharp minimum in the spectrum near 2900 nm and decreased intensity at wavelengths longer than 2900 nm suggests that these midinfrared wavelengths are not efficiently transmitted through the waveguides. This loss is likely due to OH absorption [50] in the SiO_2 since a significant fraction of the mode extends outside the AlN waveguide and into the SiO_2 cladding at these wavelengths. In the future, the use of a different cladding material could increase the output of

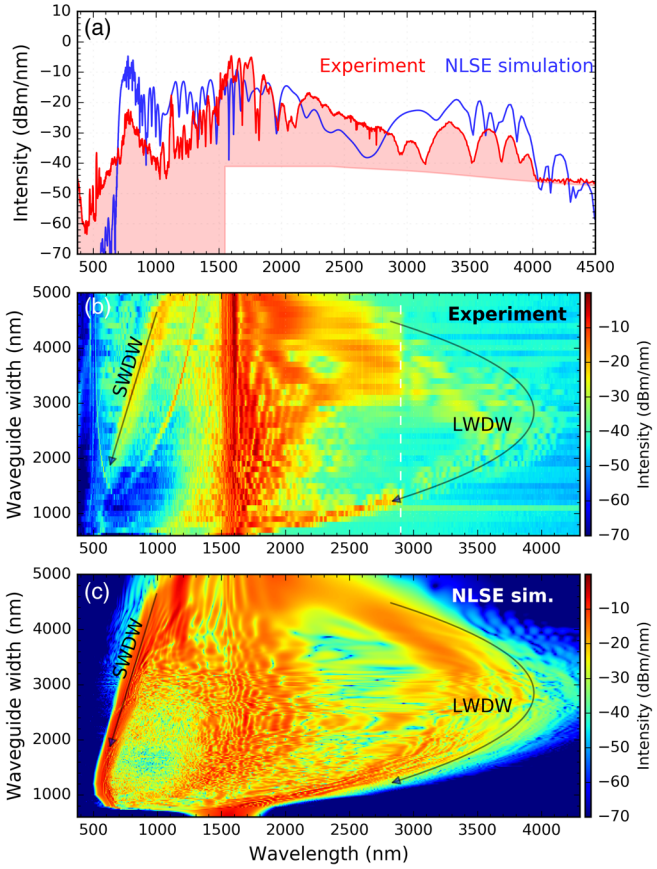

FIG. 2. Supercontinuum generation from the lowest-order quasi-transverse-electric (TE_{00}) mode. (a) Experimental and theoretical optical spectrum from the 3200-nm-wide wave-guide (scaled by +7 dB to compensate for output coupling to multimode fiber). The bottom of the shaded region indicates the noise floor of the OSA. (b) Experimentally observed spectra from all waveguide widths on the chip. The dashed line at 2900 nm indicates the onset of long-wavelength absorption in the waveguides. (c) Simulated spectra using the nonlinear Schrödinger equation (NLSE) are in general agreement with the experiment, and they suggest that wavelength-dependent absorption is decreasing the amount of midinfrared light observed experimentally. Solid lines indicate the short- and long-wavelength dispersive waves (SWDW and LWDW, respectively), and they are in the same location in both (b) and (c).

midinfrared light. Nevertheless, the waveguides still produce usable, broadband light in the midinfrared region; for example, we estimate that the 2600-nm waveguide produces about 0.3 mW in the 3500- to 4000-nm spectral region, which is sufficient power for some applications [51,52]. Indeed, the midinfrared light is easily seen in Fig. 2(b), which presents spectra collected with just a few seconds of integration time for each spectrum.

B. Brightness enhancement via a mode crossing

In the 800- to 1200-nm region, a sharp peak is seen in the supercontinuum spectrum for waveguide widths >1500 nm [Figs. 2(b) and 3(c)], which is not explained

by the NLSE. The location of the peak occurs at the wavelength where the refractive index of the lowest-order TE mode (TE_{00}) and a higher-order quasi-TM mode (TM_{10}) cross [Fig. 3(a)]. While such mode crossings are commonplace in Kerr-comb generation in microring resonators [53–55], they are not typically seen in supercontinuum generation in straight waveguides because the TE_{00} usually has the highest effective index at all wavelengths. In the case of AlN waveguides, the polarization-mode crossing occurs because AlN is a birefringent material, and the bulk index for the vertical (TM) polarization is higher than that for the horizontal (TE) polarization. At short wavelengths, where the waveguide geometry provides only a small modification to the refractive index, the TM modes tend to have the highest effective index. However, at longer wavelengths, geometric dispersion plays a larger role, lowering the effective index of the TM modes more than the TE modes and causing the polarization-mode crossing. Similarly, since modifications of the waveguide width tend to change the effective index of the TE modes more than the TM modes, the spectral location of the mode crossing also depends on the width of the waveguide [Fig. 3(b)].

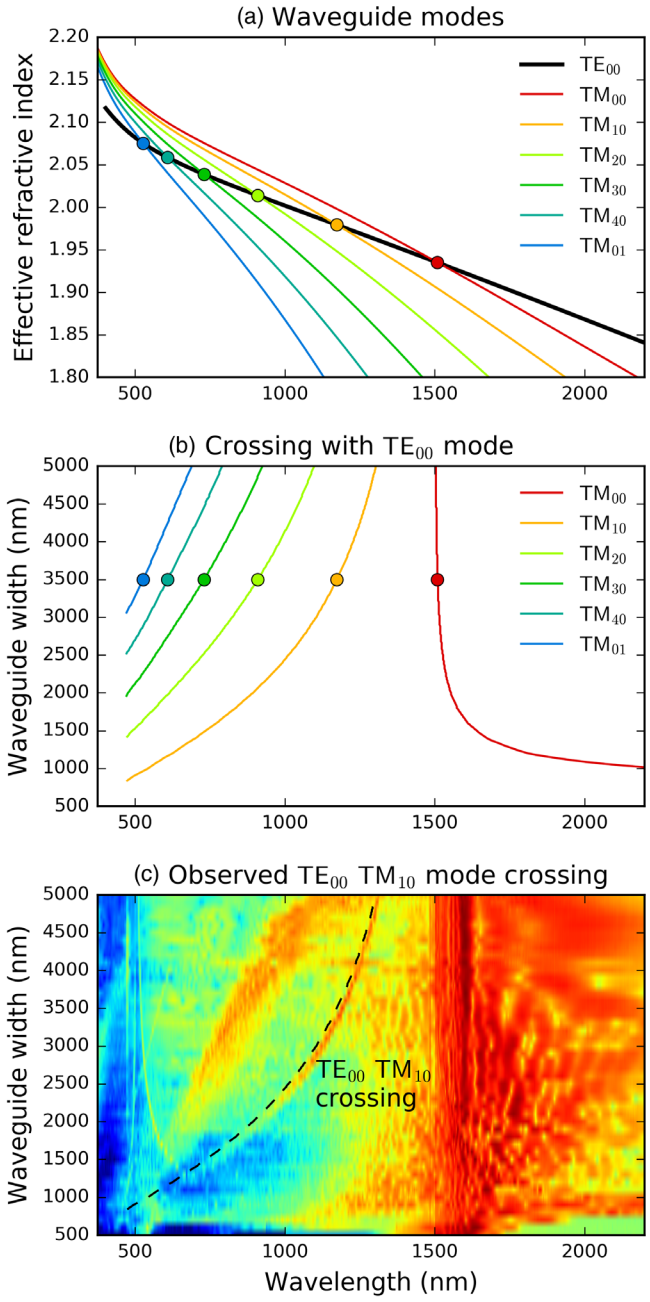

FIG. 3. (a) As the wavelength increases, the refractive index of the fundamental TE mode (TE_{00}) crosses several TM modes. A waveguide width of 3500 nm is shown. (b) The spectral location of these polarization-mode crossings changes as a function of the waveguide width (shown) and thickness (not shown). (c) The crossing of the TE_{00} and TM_{01} modes (as calculated from only the bulk refractive index and the waveguide geometry) matches the location of the sharp peak in the experimental spectra.

A mode crossing causes a sharp feature in the GVD, which can allow for the phase matching of four-wave-mixing processes in spectral regions that would otherwise be phase mismatched [53,54]. Indeed, the crossing of the TE_{00} and TM_{10} modes enables a strong enhancement of the supercontinuum spectrum in a spectral region that is otherwise dim. In some cases, this mode crossing enables an enhancement of the spectral intensity by more than 20 dB. This enhancement enables an additional amount of control over the spectral output, providing a narrow, bright region that could, for example, be used to measure a heterodyne beat with a narrow-band atomic-clock laser. It is not clear why the crossing with the TM_{10} mode is clearly seen in the experiment, while the crossings with the higher-order TM modes are absent. Understanding which mechanism couples the modes—and how this coupling could be enhanced—would allow for further customization of the spectral output of this supercontinuum source.

C. Second-harmonic generation and difference-frequency generation

Since AlN has $\chi^{(2)}$ nonlinearity, it is capable of three-wave-mixing processes, such as DFG, sum-frequency generation, and SHG. The thin AlN films used in this study are not single crystals but instead consist of many hexagonal columns, which have the crystal z axis oriented in the same (vertical) direction [40], but a random orientation for the other crystal axes. Consequently, while there is a strong $\chi^{(2)}$ component in the vertical (TM) direction, the $\chi^{(2)}$ in the horizontal (TE) direction is much weaker.

Indeed, we observe the strongest $\chi^{(2)}$ effects with the laser in the TM_{00} mode. The brightest SHG results from situations where the phase velocity of the second harmonic in a higher-order mode is the same as the phase velocity of the fundamental wavelength in the lowest-order mode. This situation provides excellent phase matching, and we observe situations where the spectral intensity of the

second-harmonic light is on the same order of magnitude as that of the transmitted pump laser [Figs. 4(a) and 4(b)]. However, this phase-matching mechanism provides a phase-matching bandwidth of only a few nanometers. Additionally, we also see third-harmonic generation (THG), which is phase matched to higher-order modes of the waveguide.

Under TM pumping, the waveguides also produce broadband light in the 3500- to 5500-nm region via DFG [Figs. 4(a) and 4(b)]. This process corresponds to the difference frequency between the spectrally broadened pump (1400–1700 nm) and the long-wavelength dispersive wave (2000–2700 nm). As the waveguide width narrows and the dispersive wave moves to shorter wavelengths, the DFG is pushed to longer wavelengths, as determined by the conservation of (photon) energy. Indeed, for waveguide widths less than 1800 nm, the DFG moves to wavelengths longer than 5500 nm, which is outside the range of our OSA. Additionally, the DFG process is strongly phase mismatched, and the conversion efficiency is therefore low. However, in principle, it is possible to achieve phase matching by launching the pump laser into a higher-order mode of the waveguide.

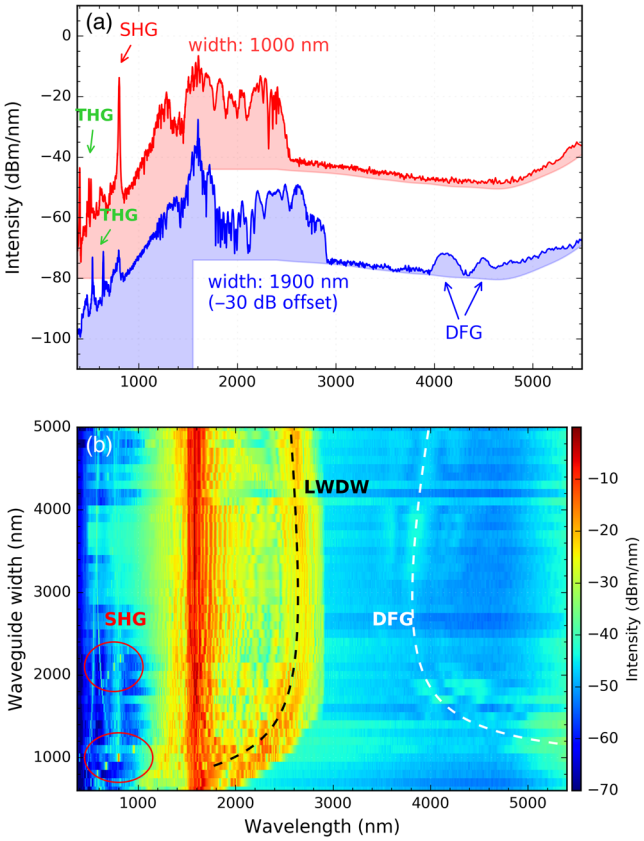

FIG. 4. Supercontinuum generation from the lowest-order quasi-transverse-magnetic (TM_{00}) mode. (a) Experimental spectra from both the 1000- and 1700-nm-wide waveguides show simultaneous supercontinuum generation, second-harmonic generation (SHG), third-harmonic generation (THG), and difference-frequency generation (DFG). (b) Experimental spectra from all waveguide widths, showing that waveguide geometry affects the positions of the long-wavelength dispersive wave (LWDW), the DFG peaks, and the phase-matched SHG peaks.

D. f_{CEO} detection and comb stabilization

Since AlN exhibits both $\chi^{(2)}$ and a strong $\chi^{(3)}$, f_{CEO} can be directly detected in the 780-nm region as a result of simultaneous SHG and SCG. Unlike a traditional f-$2f$ measurement, no interferometer is needed to set the temporal overlap of the interfering beams, and no additional alignment is necessary. The only equipment required to detect f_{CEO} is a 780-nm bandpass filter and a photodetector. Since these AlN waveguides have the strongest $\chi^{(2)}$ tensor component in the vertical direction, we observe the highest signal-to-noise ratio f_{CEO} signal when pumping in the TM_{00} mode. When TM pumping the 4800-nm-width waveguide, we achieve a 37-dB SNR for the f_{CEO} peak [Fig. 5(a)]. Interestingly, the highest SNR f_{CEO} is obtained from phase-mismatched SHG in the larger width waveguides, despite the fact that much higher efficiency phase-matched SHG is seen for waveguide widths near 1000 nm.

We speculate that the poor mode overlap between the supercontinuum (in the TM_{00} mode) and the phase-matched second harmonic (in a higher-order TM mode) hinders detection of the f_{CEO}. Indeed, a recent attempt to detect a f-$3f$ signal in SiN waveguides found that mode overlap severely limits the achievable SNR [56]. In contrast, the phase-mismatched SHG that takes place in the fundamental mode compensates for low conversion efficiency with better overlap with the supercontinuum light. Furthermore, the highest SHG conversion likely takes place at the point of soliton fission, where the pulse is compressed and the peak intensity is the highest. This is the same point where most of the supercontinuum light is generated. Since the f and $2f$ signals are generated simultaneously and propagate in the same waveguide mode, temporal overlap is provided automatically. Nevertheless, in future implementations, on-chip mode converters [57] could be used to provide both phase-matched SHG and mode overlap, thereby providing a higher f_{CEO} signal.

With the f_{CEO} detected directly from the waveguide output [Fig. 1(b)], we can achieve glitch-free f_{CEO} locking of a compact frequency comb for several hours [Fig. 5(b)]. By recording the frequency of the f_{CEO} beat with an independent Π-type [58] frequency counter [Fig. 5(c)], we can verify that the f_{CEO} has been stabilized to a level comparable to what can be achieved with a traditional f-$2f$ interferometer [41]. Unfortunately, thermal drifts in the input coupling prevent locking for more than a few hours without realignment. In the future, input and output coupling could be accomplished via fibers glued to the facets of the chip [59], which would effectively eliminate thermal drift in the coupling and enable long-term stabilization of the laser comb.

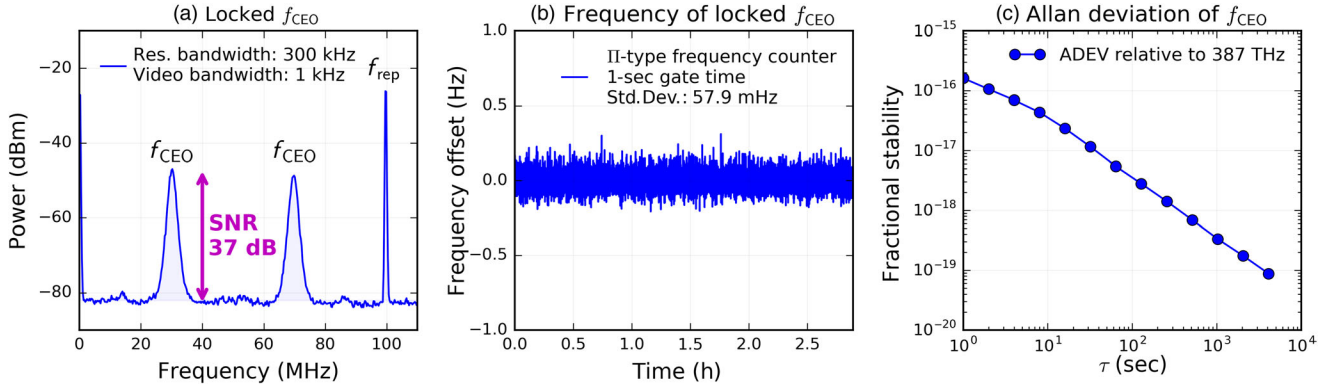

FIG. 5. (a) When the approximately 780-nm region of the supercontinuum is detected with a photodiode, the f_{CEO} can be observed directly, without the need for an interferometer. (b) The frequency of the locked f_{CEO} is stable over many hours. (c) The (ordinary) Allan deviation (ADEV) of the frequencies shown in (b) demonstrates that the comb has been stabilized to a level suitable for precision metrology.

IV. CONCLUSION

In this paper, we demonstrate aluminum nitride, a lithographically compatible material with strong $\chi^{(2)}$ and $\chi^{(3)}$ nonlinearities, as a promising material for on-chip supercontinuum generation and frequency comb self-referencing. Broadband light from 500 to 4000 nm can be generated with only about 80 mW (0.8 nJ) of 1560-nm pump power in the waveguide. Aluminum nitride provides an unexpected level of control over the output spectrum. Specifically, the birefringence of the material enables a crossing of the TE and TM modes, which provides an enhancement in the spectral intensity by several orders of magnitude. In addition, we observe phase-mismatched difference-frequency generation across the 3500- to 5500-nm region, which, if phase matched, could provide a useful midinfrared light source. Moreover, fully phase matched second- and third-harmonic generation provide narrow-band light that is tunable across the visible region.

Simultaneous second-harmonic and supercontinuum generation processes allow for the simplified detection of f_{CEO} using a single, monolithic waveguide and enable high-quality stabilization of a compact laser frequency comb. In conclusion, aluminum nitride waveguides provide both robust comb stabilization and access to broad spectra across the visible, near-infrared, and midinfrared regions. These capabilities are crucial ingredients for building inexpensive, portable frequency combs for field applications such as dual-comb spectroscopy, spectrograph calibration, and precision metrology.

ACKNOWLEDGMENTS

The authors thank Nima Nader, Jeff Chiles, Frank Quinlan, and Tara Fortier for the helpful discussions and acknowledge assistance in device fabrication provided by Yale clean-room staff Michael Power and Michael Rooks. This material is based upon work supported by the Air Force Office of Scientific Research under Grant No. FA9550-16-1-0016, the Defense Advanced Research Projects Agency (DARPA) ACES, PULSE, and SCOUT programs, the National Aeronautics and Space Administration (NASA), the National Institute of Standards and Technology (NIST), the National Research Council (NRC), and the National Science Foundation (NSF) Graduate Research Fellowship Program (GRFP).

Contributions to this article by workers at NIST, an agency of the U.S. Government, are not subject to U.S. copyright.

[1] T. Rosenband, D. B. Hume, P. O. Schmidt, C. W. Chou, A. Brusch, L. Lorini, W. H. Oskay, R. E. Drullinger, T. M. Fortier, J. E. Stalnaker, S. A. Diddams, W. C. Swann, N. R. Newbury, W. M. Itano, D. J. Wineland, and J. C. Bergquist, Frequency ratio of Al^+ and Hg^+ single-ion optical clocks; metrology at the 17th decimal place, Science **319**, 1808 (2008).

[2] G. B. Rieker, F. R. Giorgetta, W. C. Swann, J. Kofler, A. M. Zolot, L. C. Sinclair, E. Baumann, C. Cromer, G. Petron, C. Sweeney, P. P. Tans, I. Coddington, and N. R. Newbury, Frequency-comb-based remote sensing of greenhouse gases over kilometer air paths, Optica **1**, 290 (2014).

[3] E. M. Waxman, K. C. Cossel, G.-W. Truong, F. R. Giorgetta, W. C. Swann, S. Coburn, R. J. Wright, G. B. Rieker, I. Coddington, and N. R. Newbury, Intercomparison of open-path trace gas measurements with two dual frequency comb spectrometers, Atmos. Meas. Tech. Discuss. **2017**, 1 (2017).

[4] Chih-Hao Li, Andrew J. Benedick, Peter Fendel, Alexander G. Glenday, Franz X. Kärtner, David F. Phillips, Dimitar Sasselov, Andrew Szentgyorgyi, and Ronald L. Walsworth, A laser frequency comb that enables radial velocity measurements with a precision of 1 cm s^{-1}, Nature (London) **452**, 610 (2008).

[5] Gabriel G. Ycas, Franklyn Quinlan, Scott A. Diddams, Steve Osterman, Suvrath Mahadevan, Stephen Redman, Ryan Terrien, Lawrence Ramsey, Chad F. Bender, Brandon

Botzer, and Steinn Sigurdsson, Demonstration of on-sky calibration of astronomical spectra using a 25 GHz near-IR laser frequency comb, Opt. Express **20**, 6631 (2012).

[6] T. J. Kippenberg, R. Holzwarth, and S. A. Diddams, Microresonator-based optical frequency combs, Science **332**, 555 (2011).

[7] John M. Dudley, Gory Genty, and Stphane Coen, Supercontinuum generation in photonic crystal fiber, Rev. Mod. Phys. **78**, 1135 (2006).

[8] David J. Jones, Scott A. Diddams, Jinendra K. Ranka, Andrew Stentz, Robert S. Windeler, John L. Hall, and Steven T. Cundiff, Carrier-envelope phase control of femtosecond mode-locked lasers and direct optical frequency synthesis, Science **288**, 635 (2000).

[9] R. Holzwarth, Th. Udem, T. W. Hänsch, J. C. Knight, W. J. Wadsworth, and P.St. J. Russell, Optical Frequency Synthesizer for Precision Spectroscopy, Phys. Rev. Lett. **85**, 2264 (2000).

[10] Scott A. Diddams, David J. Jones, Jun Ye, Steven T. Cundiff, John L. Hall, Jinendra K. Ranka, Robert S. Windeler, Ronald Holzwarth, Thomas Udem, and T. W. Hänsch, Direct Link between Microwave and Optical Frequencies with a 300 THz Femtosecond Laser Comb, Phys. Rev. Lett. **84**, 5102 (2000).

[11] T. Kobayashi, T Sueta, Y. Cho, and Y. Matsu, High-repetition-rate optical pulse generator using a Fabry-Perot electro-optic modulator, Appl. Phys. Lett. **21**, 341 (1972).

[12] Victor Torres-Company and Andrew M. Weiner, Optical frequency comb technology for ultra-broadband radio-frequency photonics, Laser Photonics Rev. **8**, 368 (2014).

[13] P. Del'Haye, A. Schliesser, O. Arcizet, T. Wilken, R. Holzwarth, and T. J. Kippenberg, Optical frequency comb generation from a monolithic microresonator, Nature (London) **450**, 1214 (2007).

[14] T. Herr, V. Brasch, J. D. Jost, C. Y. Wang, N. M. Kondratiev, M. L. Gorodetsky, and T. J. Kippenberg, Temporal solitons in optical microresonators, Nat. Photonics **8**, 145 (2014).

[15] Albert Schliesser, Nathalie Picque, and Theodor W. Hansch, Mid-infrared frequency combs, Nat. Photonics **6**, 440 (2012).

[16] Ian Coddington, Nathan Newbury, and William Swann, Dual-comb spectroscopy, Optica **3**, 414 (2016).

[17] Gar-Wing Truong, Eleanor Waxman, Kevin C. Cossel, Fabrizio Giorgetta, William C. Swann, Ian R. Coddington, and Nathan R. Newbury, Dual-comb Spectroscopy for City-scale Open Path Greenhouse Gas Monitoring, in *Proceedings of the Conference on Lasers and Electro-Optics, San Jose, 2016* (Optical Society of America, Washington, DC, 2016), p. SW4H.2.

[18] Fabrizio R. Giorgetta, Gregory B. Rieker, Esther Baumann, William C. Swann, Laura C. Sinclair, Jon Kofler, Ian Coddington, and Nathan R. Newbury, Broadband Phase Spectroscopy over Turbulent Air Paths, Phys. Rev. Lett. **115**, 103901 (2015).

[19] Kevin C. Cossel, Eleanor M. Waxman, Ian A. Finneran, Geoffrey A. Blake, Jun Ye, and Nathan R. Newbury, Gas-phase broadband spectroscopy using active sources: Progress, status, and applications, J. Opt. Soc. Am. B **34**, 104 (2017).

[20] Jorn P. Epping, Tim Hellwig, Marcel Hoekman, Richard Mateman, Arne Leinse, Ren G. Heideman, Albert van Rees, Peter J. M. van der Slot, Chris J. Lee, Carsten Fallnich, and Klaus-J. Boller, On chip visible-to-infrared supercontinuum generation with more than 495 THz spectral bandwidth, Opt. Express **23**, 19596 (2015).

[21] Marco A. G. Porcel, Florian Schepers, Jörn P. Epping, Tim Hellwig, Marcel Hoekman, René G. Heideman, Peter J. M. van der Slot, Chris J. Lee, Robert Schmidt, Rudolf Bratschitsch, Carsten Fallnich, and Klaus-J. Boller, Two-octave spanning supercontinuum generation in stoichiometric silicon nitride waveguides pumped at telecom wavelengths, Opt. Express **25**, 1542 (2017).

[22] Alexander Klenner, Aline S. Mayer, Adrea R. Johnson, Kevin Luke, Michael R. E. Lamont, Yoshitomo Okawachi, Michal Lipson, Alexander L. Gaeta, and Ursula Keller, Gigahertz frequency comb offset stabilization based on supercontinuum generation in silicon nitride waveguides, Opt. Express **24**, 11043 (2016).

[23] A. S. Mayer, A. Klenner, A. R. Johnson, K. Luke, M. R. E. Lamont, Y. Okawachi, M. Lipson, A. L. Gaeta, and U. Keller, Frequency comb offset detection using supercontinuum generation in silicon nitride waveguides, Opt. Express **23**, 15440 (2015).

[24] J. M. Chavez Boggio, D. Bodenmller, T. Fremberg, R. Haynes, M. M. Roth, R. Eisermann, M. Lisker, L. Zimmermann, and M. Bhm, Dispersion engineered silicon nitride waveguides by geometrical and refractive-index optimization, J. Opt. Soc. Am. B **31**, 2846 (2014).

[25] Daniel Hickstein, Gabriel Ycas, Alex Lind, Daniel C. Cole, Katrik Srinivasan, Scott Diddams, and Scott Papp, Photonic-chip Waveguides for Supercontinuum Generation with Picojoule Pulses, in *Proceedings of the Advanced Photonics Conference, Vancouver, Canada, 2016* (Optical Society of America, Washington, DC, 2016), p. IM3A.2.

[26] David Carlson, Daniel Hickstein, Alexander Lind, Judith Olson, Richard Fox, Roger Brown, Andrew Ludlow, Qing Li, Daron Westly, Holly Leopardi, Tara Fortier, Kartik Srinivasan, Scott Diddams, and Scott Papp, Photonic-chip supercontinuum with tailored spectra for counting optical frequencies, arXiv:1702.03269 [Phys. Rev. Applied (to be published)].

[27] Adrea R. Johnson, Aline S. Mayer, Alexander Klenner, Kevin Luke, Erin S. Lamb, Michael R. E. Lamont, Chaitanya Joshi, Yoshitomo Okawachi, Frank W. Wise, Michal Lipson, Ursula Keller, and Alexander L. Gaeta, Octave-spanning coherent supercontinuum generation in a silicon nitride waveguide, Opt. Lett. **40**, 5117 (2015).

[28] Neetesh Singh, Darren D. Hudson, Yi Yu, Christian Grillet, Stuart D. Jackson, Alvaro Casas-Bedoya, Andrew Read, Petar Atanackovic, Steven G. Duvall, Stefano Palomba, Barry Luther-Davies, Stephen Madden, David J. Moss, and Benjamin J. Eggleton, Midinfrared supercontinuum generation from 2 to 6 μm in a silicon nanowire, Optica **2**, 797 (2015).

[29] I.-Wei Hsieh, Xiaogang Chen, Xiaoping Liu, Jerry I. Dadap, Nicolae C. Panoiu, Cheng-Yun Chou, Fengnian Xia, William M. Green, Yurii A. Vlasov, and Richard M. Osgood, Supercontinuum generation in silicon photonic wires, Opt. Express **15**, 15242 (2007).

[30] Franois Leo, Simon-Pierre Gorza, Stphane Coen, Bart Kuyken, and Gunther Roelkens, Coherent supercontinuum generation in a silicon photonic wire in the telecommunication wavelength range, Opt. Lett. **40**, 123 (2015).

[31] Minhao Pu, Hua Ji, Hao Hu, Luisa Ottaviano, Elizaveta Semenova, Pengyu Guan, Leif K. Oxenløwe, and Kresten Yvind, Supercontinuum Generation in AlGaAs-On-Insulator Nano-Waveguide at Telecom Wavelengths, in *Proceedings of the Conference on Lasers and Electro-Optics, San Jose, 2016* (Optical Society of America, Washington, DC, 2016), p. AM3J.3.

[32] Yi Yu, Xin Gai, Ting Wang, Pan Ma, Rongping Wang, Zhiyong Yang, Duk-Yong Choi, Steve Madden, and Barry Luther-Davies, Mid-infrared supercontinuum generation in chalcogenides, Opt. Mater. Express **3**, 1075 (2013).

[33] Michael R. E. Lamont, Barry Luther-Davies, Duk-Yong Choi, Steve Madden, and Benjamin J. Eggleton, Supercontinuum generation in dispersion engineered highly nonlinear ($\gamma = 10/\mathrm{W/m}$) As_2S_3 chalcogenide planar waveguide, Opt. Express **16**, 14938 (2008).

[34] Kana Iwakuni, Sho Okubo, Osamu Tadanaga, Hajime Inaba, Atsushi Onae, Feng-Lei Hong, and Hiroyuki Sasada, Generation of a frequency comb spanning more than 3.6 octaves from ultraviolet to mid infrared, Opt. Lett. **41**, 3980 (2016).

[35] Hairun Guo, Binbin Zhou, Michael Steinert, Frank Setzpfandt, Thomas Pertsch, Hung-ping Chung, Yen-Hung Chen, and Morten Bache, Supercontinuum generation in quadratic nonlinear waveguides without quasi-phase matching, Opt. Lett. **40**, 629 (2015).

[36] Carsten Langrock, M. M. Fejer, I. Hartl, and Martin E. Fermann, Generation of octave-spanning spectra inside reverse-proton-exchanged periodically poled lithium niobate waveguides, Opt. Lett. **32**, 2478 (2007).

[37] Xiang Guo, Chang-Ling Zou, and Hong X. Tang, Second-harmonic generation in aluminum nitride microrings with 2500%/W conversion efficiency, Optica **3**, 1126 (2016).

[38] Hojoong Jung, Chi Xiong, King Y. Fong, Xufeng Zhang, and Hong X. Tang, Optical frequency comb generation from aluminum nitride microring resonator, Opt. Lett. **38**, 2810 (2013).

[39] S. Zhao, A. T. Connie, M. H. T. Dastjerdi, X. H. Kong, Q. Wang, M. Djavid, S. Sadaf, X. D. Liu, I. Shih, H. Guo, and Z. Mi, Aluminum nitride nanowire light emitting diodes: Breaking the fundamental bottleneck of deep ultraviolet light sources, Sci. Rep. **5**, 8332 (2015).

[40] Chi Xiong, Wolfram H. P. Pernice, and Hong X. Tang, Low-loss, silicon integrated, aluminum nitride photonic circuits and their use for electro-optic signal processing, Nano Lett. **12**, 3562 (2012).

[41] L. C. Sinclair, J.-D. Deschnes, L. Sonderhouse, W. C. Swann, I. H. Khader, E. Baumann, N. R. Newbury, and I. Coddington, A compact optically coherent fiber frequency comb, Rev. Sci. Instrum. **86**, 081301 (2015).

[42] J. Hult, A fourth-order Runge-Kutta in the interaction picture method for simulating supercontinuum generation in optical fibers, J. Lightwave Technol. **25**, 3770 (2007).

[43] A. M. Heidt, Efficient adaptive step size method for the simulation of supercontinuum generation in optical fibers, J. Lightwave Technol. **27**, 3984 (2009).

[44] Gabriel Ycas, Daniel Maser, and Daniel D. Hickstein, pyNLO—Nonlinear optics modeling for Python, https://github.com/pyNLO/PyNLO.

[45] A. A. Amorim, M. V. Tognetti, P. Oliveira, J. L. Silva, L. M. Bernardo, F. X. Kärtner, and H. M. Crespo, Sub-two-cycle pulses by soliton self-compression in highly nonlinear photonic crystal fibers, Opt. Lett. **34**, 3851 (2009).

[46] A. B. Fallahkhair, K. S. Li, and T. E. Murphy, Vector finite difference modesolver for anisotropic dielectric waveguides, J. Lightwave Technol. **26**, 1423 (2008).

[47] Ikeda *et al.*, Thermal and Kerr nonlinear properties of plasma-deposited silicon nitride/silicon dioxide waveguides, Optics Express **16**, 12987 (2008).

[48] Nail Akhmediev and Magnus Karlsson, Cherenkov radiation emitted by solitons in optical fibers, Phys. Rev. A **51**, 2602 (1995).

[49] T. W. Graham Solomons and Craig B. Fryhle, *Organic Chemistry*, 10th ed. (Wiley, New York, 2009).

[50] G. Navarra, I. Iliopoulos, V. Militello, S. G. Rotolo, and M. Leone, OH-related infrared absorption bands in oxide glasses, J. Non-Cryst. Solids **351**, 1796 (2005).

[51] Daniel L. Maser, Gabriel Ycas, William I. Depetri, Flavio C. Cruz, and Scott A. Diddams, Coherent frequency combs for spectroscopy across the 35 m region, Appl. Phys. B **123**, 142 (2017).

[52] Nima Nader, Daniel L. Maser, Daniel L. Maser, Flavio C. Cruz, Connor Fredrick, Connor Fredrick, Gabriel Ycas, Daron Westly, Richard Mirin, Jeffrey Shainline, Scott Diddams, and Scott Diddams, Coherent On-Chip Spectral-Engineered Mid-IR Frequency Comb Generation in Si Waveguides, in *Proceedings of the Conference on Lasers and Electro-Optics, San Jose, 2017* (Optical Society of America, Washington, DC, 2017), p. FTu3D.4.

[53] Daniel C. Cole, Erin S. Lamb, Pascal Del'Haye, Scott A. Diddams, and Scott B. Papp, Soliton crystals in Kerr resonators, arXiv:1610.00080.

[54] Sven Ramelow, Alessandro Farsi, Stphane Clemmen, Jacob S. Levy, Adrea R. Johnson, Yoshitomo Okawachi, Michael R. E. Lamont, Michal Lipson, and Alexander L. Gaeta, Strong polarization mode coupling in microresonators, Opt. Lett. **39**, 5134 (2014).

[55] T. Herr, V. Brasch, J. D. Jost, I. Mirgorodskiy, G. Lihachev, M. L. Gorodetsky, and T. J. Kippenberg, Mode Spectrum and Temporal Soliton Formation in Optical Microresonators, Phys. Rev. Lett. **113**, 123901 (2014).

[56] David R. Carlson, Daniel D. Hickstein, Alex Lind, Stefan Droste, Daron Westly, Nima Nader, Ian Coddington, Nathan R. Newbury, Kartik Srinivasan, Scott A. Diddams, and Scott B. Papp, Self-referenced frequency combs using high-efficiency silicon-nitride waveguides, Opt. Lett. **42**, 2314 (2017).

[57] Xiang Guo, Chang-Ling Zou, Hojoong Jung, and Hong X. Tang, On Chip Strong Coupling and Efficient Frequency Conversion between Telecom and Visible Optical Modes, Phys. Rev. Lett. **117**, 123902 (2016).

[58] S. T. Dawkins, J. J. McFerran, and A. N. Luiten, Considerations on the measurement of the stability of oscillators with frequency counters, IEEE Trans. Ultrason. Ferroelectr. Freq. Control **54**, 918 (2007).

[59] Hojoong Jung, Xiang Guo, Na Zhu, Scott B. Papp, Scott A. Diddams, and Hong X. Tang, Phase-dependent interference between frequency doubled comb lines in a $\chi^{(2)}$ phase-matched aluminum nitride microring, Opt. Lett. **41**, 3747 (2016).